LETTER

doi:10.1038/nature20135

# The evolving quality of frictional contact with graphene

Suzhi Li[1,2,3], Qunyang Li[4,5], Robert W. Carpick[6], Peter Gumbsch[7,8], Xin Z. Liu[6], Xiangdong Ding[1], Jun Sun[1,9] & Ju Li[1,2,9]

**Graphite and other lamellar materials are used as dry lubricants for macroscale metallic sliding components and high-pressure contacts. It has been shown experimentally that monolayer graphene exhibits higher friction than multilayer graphene and graphite, and that this friction increases with continued sliding, but the mechanism behind this remains subject to debate. It has long been conjectured that the true contact area between two rough bodies controls interfacial friction[1]. The true contact area, defined for example by the number of atoms within the range of interatomic forces, is difficult to visualize directly but characterizes the quantity of contact. However, there is emerging evidence that, for a given pair of materials, the quality of the contact can change, and that this can also strongly affect interfacial friction[2–7]. Recently, it has been found that the frictional behaviour of two-dimensional materials exhibits traits[8–13] unlike those of conventional bulk materials. This includes the abovementioned finding that for few-layer two-dimensional materials the static friction force gradually strengthens for a few initial atomic periods before reaching a constant value. Such transient behaviour, and the associated enhancement of steady-state friction, diminishes as the number of two-dimensional layers increases, and was observed only when the two-dimensional material was loosely adhering to a substrate[8]. This layer-dependent transient phenomenon has not been captured by any simulations[14,15]. Here, using atomistic simulations, we reproduce the experimental observations of layer-dependent friction and transient frictional strengthening on graphene. Atomic force analysis reveals that the evolution of static friction is a manifestation of the natural tendency for thinner and less-constrained graphene to re-adjust its configuration as a direct consequence of its greater flexibility. That is, the tip atoms become more strongly pinned, and show greater synchrony in their stick–slip behaviour. While the quantity of atomic-scale contacts (true contact area) evolves, the quality (in this case, the local pinning state of individual atoms and the overall commensurability) also evolves in frictional sliding on graphene. Moreover, the effects can be tuned by pre-wrinkling. The evolving contact quality is critical for explaining the time-dependent friction of configurationally flexible interfaces.**

We conducted molecular dynamics simulations by sliding a silicon tip over graphene supported on an amorphous Si (a-Si) substrate (see Methods). Substrate–graphene adhesion was modelled as a van der Waals interaction with an effective work of adhesion of approximately 0.1 J m$^{-2}$, based on experimental values[16]. Figure 1a shows the relaxed system consisting of a-Si and a monolayer of graphene at 300 K. As in experiments[16], the modelled surface morphology of graphene conformed well to the a-Si substrate (Fig. 1b and c). A rigid round $\langle 001 \rangle$-oriented crystalline silicon tip with a radius of 16.3 nm was placed in contact with graphene (Fig. 1d) and equilibrated for 2 ns (Fig. 1e and f). Graphene's high out-of-plane flexibility coupled with tip–graphene adhesion causes local puckering near the contact edge (Fig. 1e, arrow). A similar puckering phenomenon was also found for the multilayer graphene systems (see Supplementary Discussion 1).

We then applied an external normal load of 0.8 nN to the tip and further relaxed the whole system. After relaxation, we displaced a harmonic spring laterally coupled to the tip at 2 m s$^{-1}$. It is noted that the normal load was stably maintained at 0.8 nN during the friction simulation (see Supplementary Discussion 2). As the tip slid on graphene (with layer numbers $N = 1$–4), clear stick–slip motion with two distinct stages was observed in all cases (Fig. 1g), in contrast to conventional atomic stick–slip on bulk graphite[17]. Initially, the local peaks of the lateral force (that is, the static friction force, when slip initiates) increased progressively with each slip. After a few periods, the behaviour became regular, and the peak forces remained constant. The slip distance in each stick–slip event is approximately 2.5 Å, equivalent to the lattice spacing of graphene. The simulations consistently reproduce, for the first time, the two-stage friction behaviour observed in experiments[8].

Our simulations also show layer-dependent friction[8], that is, the strengthening effect became weaker and the frictional force reduced as sample thickness increased; the strengthening almost vanished once the thickness reached four layers. To check that two-stage friction was not a dynamic effect caused by the high sliding speed, we first reduced the speed to 1 m s$^{-1}$ and 0.5 m s$^{-1}$ and found that there is only a weak dependence of the frictional strengthening on sliding speed (see Supplementary Discussion 3). In addition, we performed quasi-static calculations[5,18] and found that the two-stage friction trait was retained (see Supplementary Discussion 4). Finally, we computed the energy barriers for stick–slip motion, and confirmed that the stick–slip event is not driven primarily by thermal fluctuations at experimental time and force scales, but primarily by the external forcing (see Supplementary Discussion 5).

Early studies attributed the friction enhancement for thinner two-dimensional samples to puckering[8,14,19], where the sliding tip induces more out-of-plane deformation for thinner samples, leading to a larger true contact area and thereby a larger friction. Here, we also observed noticeable puckering (Fig. 1e, Supplementary Video) and found that the puckered configuration evolved as the tip moved forward. Figure 1h shows the average friction force together with the contact area in the constant static friction force regime (that is, beyond the initial strengthening regime) for different layered graphene samples. The simulations show that a larger contact area corresponded to larger friction, and was correlated with increased puckering. However, the friction increase

[1]State Key Laboratory for Mechanical Behavior of Materials and Frontier Institute of Science and Technology, Xi'an Jiaotong University, Xi'an 710049, China. [2]Department of Nuclear Science and Engineering and Department of Materials Science and Engineering, Massachusetts Institute of Technology, Cambridge, Massachusetts 02139, USA. [3]Institute of Nanotechnology, Karlsruhe Institute of Technology, 76344 Eggenstein-Leopoldshafen, Germany. [4]Center for Nano and Micro Mechanics, Applied Mechanics Laboratory, School of Aerospace Engineering, Tsinghua University, Beijing 100084, China. [5]State Key Laboratory of Tribology, Tsinghua University, Beijing 100084, China. [6]Department of Mechanical Engineering and Applied Mechanics, University of Pennsylvania, Philadelphia, Pennsylvania 19104, USA. [7]Institute for Applied Materials, Karlsruhe Institute of Technology, 76131 Karlsruhe, Germany. [8]Fraunhofer Institute for Mechanics of Materials IWM, 79108 Freiburg, Germany. [9]Center for Advancing Materials Performance from the Nanoscale (CAMP-Nano), School of Materials Science and Engineering, Xi'an Jiaotong University, Xi'an 710049, China.

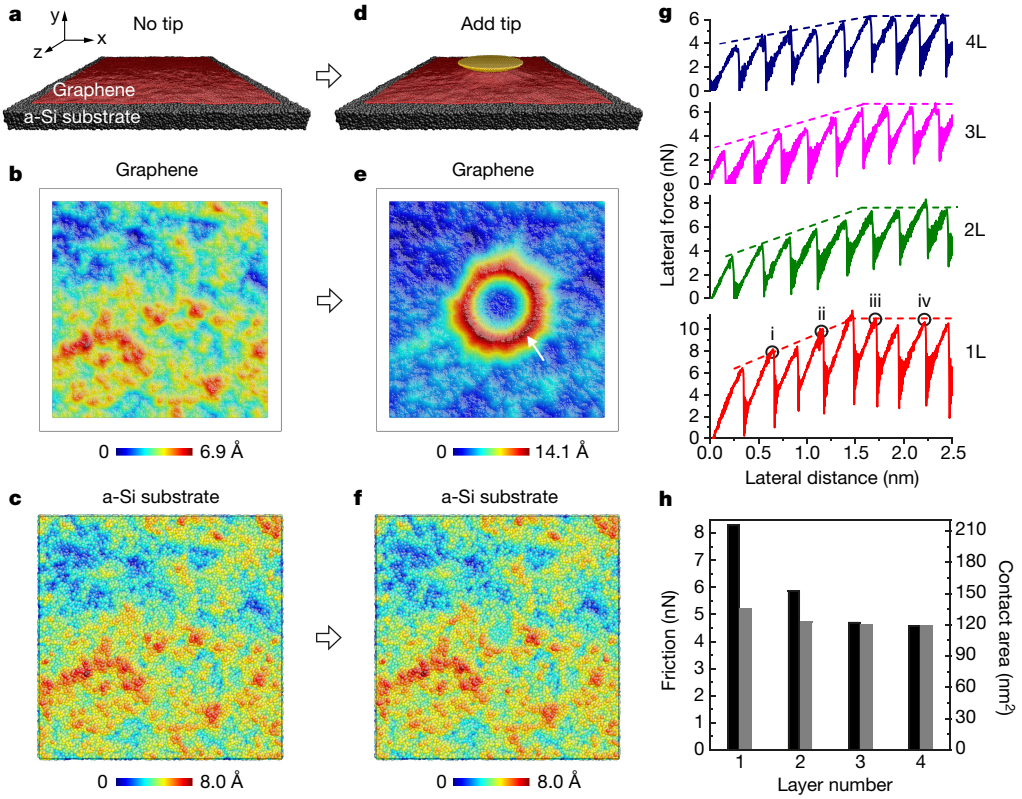


**Figure 1 | Model setup and frictional behaviour for a Si tip sliding over a graphene/a-Si substrate system at 300 K. a**, Graphene adhering to the a-Si substrate. **b**, **c**, Surface morphology of monolayer graphene (**b**) and the substrate (**c**). **d**, A rigid Si tip is placed in contact with graphene for the friction tests. **e**, **f**, Morphology of monolayer graphene (**e**) and substrate (**f**) in the presence of the tip after 2 ns. The lateral dimensions of the substrate and graphene are 43.4 nm × 43.4 nm and 38.5 nm × 38.6 nm, respectively. **g**, Force traces showing stick–slip behaviour on single (1L) and multilayer (2L–4L) graphene/a-Si substrates. **h**, Variations of averaged friction (black) and contact area (grey) with number of layers of graphene. The black, red and gold atoms in **a** and **d** refer to the a-Si substrate, graphene and the tip, respectively; atoms in **b**, **c**, **e** and **f** are coloured according to the height amplitude along the *y* direction. The tip–graphene contact area is taken to be *ms*, where *m* is the number of graphene atoms that are in intimate contact with the tip atoms and *s* (2.77 Å$^2$ per atom) is the atomic area of graphene (see Methods for details).

(an 80% increase for monolayer versus four-layer graphene, consistent with experiments) was substantially larger than the change in contact area (14%). Therefore, the true contact area (which by definition is geometric and additive) change caused by the puckering of graphene alone cannot account for the large increase in friction. This strongly suggests the existence of additional mechanisms contributing to the layer dependence of friction and the transient strengthening.

To trace the physical processes at play, we analysed the distribution of atomistic interaction forces at the interface. For the tip, the net lateral interaction force from graphene, $F_{\text{interact}}$, is the sum of the $x$ components of all atomic forces exerted by graphene, $F_{\text{interact}} = \sum_i f_i^{\text{friction}} = \sum_i (f_i(x_{\text{spr}}) - f_i(0))$, where $f_i(x_{\text{spr}})$ is the $x$ component of the graphene–tip interaction force for tip atom $i$ when the spring moves a distance $x_{\text{spr}}$, and $f_i(0)$ is the interaction force before sliding. To highlight the resultant forces due to sliding, we considered only the incremental interfacial forces with respect to the initial state (see Supplementary Discussion 6).

We first performed interfacial force analysis for monolayer graphene. Figure 2a–d shows the $f_i^{\text{friction}}$ distributions at four moments, each when the lateral force reached its local peak values during the stick–slip friction, marked i, ii, iii and iv in Fig. 1g. Owing to the crystallographic and geometrical differences between graphene and silicon, $f_i^{\text{friction}}$ values at all four moments exhibited a seemingly random distribution; the total sum in each case was negative (thus producing frictional resistance). The $f_i^{\text{friction}}$ distribution clearly evolved from points i to iii (Fig. 2a–c) and was almost unchanged between points iii and iv (Fig. 2c and d).

We individually followed $f_i^{\text{friction}}$ of a few tip atoms that were acting as pinning sites or 'traps' (see Supplementary Discussion 7). For some of these atoms, the absolute value of $f_i^{\text{friction}}$ increased in the strengthening stage and then saturated. This indicates that pinning gets progressively stronger at these sites with each slip. These atoms apparently provide a substantial contribution to frictional strengthening. For most atoms, the variation of $f_i^{\text{friction}}$ was steady, indicating no pinning enhancement. These atoms contribute to the overall friction, but not to the initial transient strengthening by local trap deepening.

Further inspection shows that the variation of the interfacial force is closely related to the local configuration of the contacting graphene. If the environment near a tip atom allows the graphene to locally adjust its atomic configuration, the interfacial force will exhibit an evolution effect. However, the detailed local contact environment varies from atom to atom owing to complex tip, graphene and rough substrate configurations. We cannot tell beforehand how an individual tip atom and its surrounding would evolve, because they not only depend on the initial configuration but also depend on the randomly rough surface and the complicated deformation history (for example, the statistical features of the final configuration depend on the entire sliding path, and not just on the initial and final tip locations). Nevertheless, our simulations clearly demonstrate that the interface tends to evolve towards a more commensurate (that is, with more atomic alignment at the interface) and better-pinned state (that is, it finds a deeper energy trap).

To quantify this, we plotted the histogram of the atomic interaction forces at these four moments in Fig. 2e. All four histograms have larger populations at low-magnitude interaction forces and much lower populations at high magnitude. However, these histograms were all skewed negatively because the overall net force was negative. More importantly, as indicated by the insets of Fig. 2e, the range of the distribution increased appreciably from points i to iv (for example, the maximum forces are around ±0.6 nN at point i, but increase to ±0.8 nN

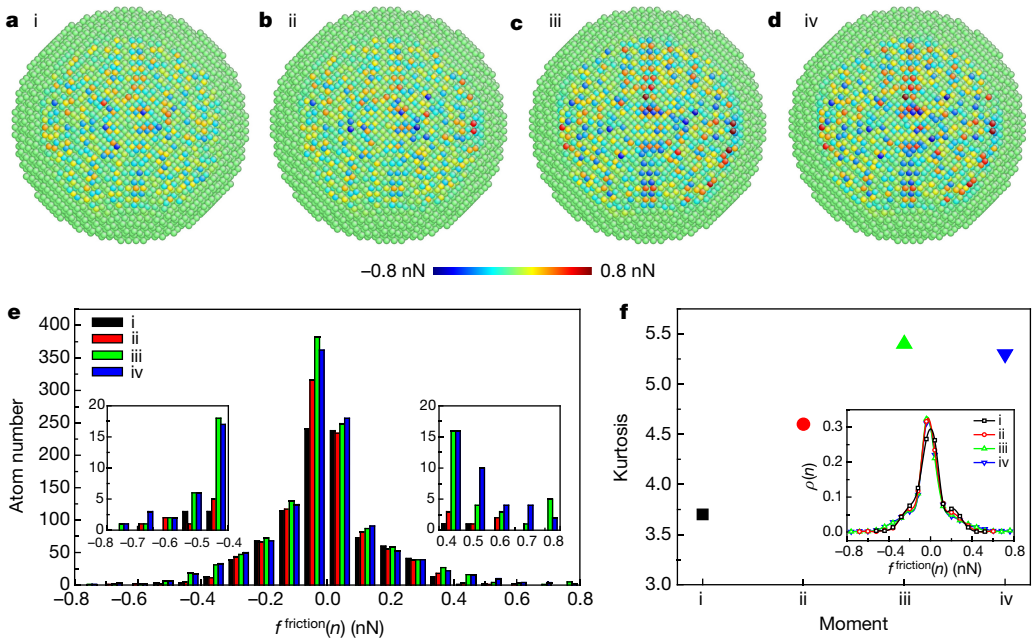


**Figure 2 | Evolution of the atomic-level forces contributing to friction on a monolayer graphene/a-Si substrate. a–d**, Corresponding $f_i^{\text{friction}}$ distribution at the four moments marked in Fig. 1g. The sites with positive magnitude of $f_i^{\text{friction}}$ (red colour) are the local pushing points that help the tip slip forward (to the right), while the sites with negative magnitude of $f_i^{\text{friction}}$ (blue colour) are the local pinning points that produce lateral resistance. **e**, The histogram of $f^{\text{friction}}(n)$ at each of the four moments. The histogram is obtained by dividing the range of interfacial forces into twenty bins and plotting the number of tip atoms with interaction forces within each bin. The insets provide a magnified view of the distribution in the tails. **f**, The kurtosis value for the four force distributions at the four moments. The inset shows the force distributions that were used to calculate kurtosis. $\rho(n)$ is the normalized atom number in each corresponding bin of interfacial forces.

at points iii and iv). This local force enhancement is consistent with the higher contrast of interfacial forces shown in Fig. 2a–d, which confirms the abovementioned local trap deepening. In addition, geometrical analysis also suggests that the tip–graphene interface evolved through small atomic shifts to produce more intimate atomic contact as the tip was displaced forward, providing more atomic pinning sites for lateral sliding (see Supplementary Discussion 8).

We further analysed the evolving commensurability of the interface. A less structured contact interface should have a unimodal force distribution, similar to a Gaussian or even a uniform distribution. A very effective parameter with which to describe the deviation from a unimodal distribution (see Supplementary Discussion 9) is the kurtosis $K = \mu_4/\sigma^4$, where $\mu_4$ is the fourth moment about the mean value and $\sigma$ is the standard deviation of the distribution (see Methods). The larger $K$, the more structured the distribution becomes, and the more commensurate the interface. Figure 2f show the kurtosis values for points i to iv. The kurtosis increased from point i to point iii and was almost unchanged between points iii and iv. This provides an

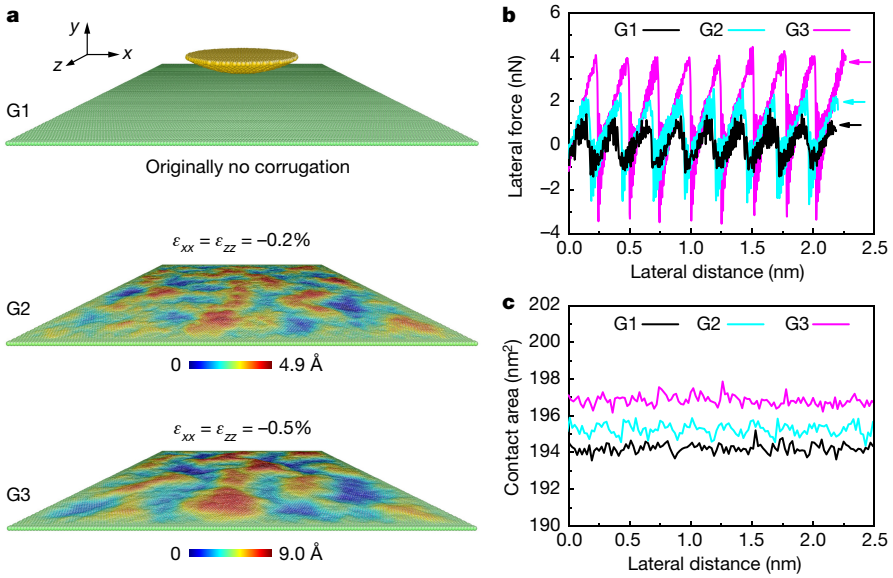


**Figure 3 | Simulations of stick–slip friction on monolayer suspended graphene at 300 K. a**, Simulation model. Three graphene samples with different amounts of pre-existing wrinkles are generated, named G1, G2 and G3. The colours represent the out-of-plane height amplitude. The induced peak-to-peak height undulations of G2 and G3 are 4.9 Å and 9.0 Å, respectively. **b**, Lateral force traces showing friction sliding on the three samples. **c**, Variation of tip–graphene contact area during sliding.

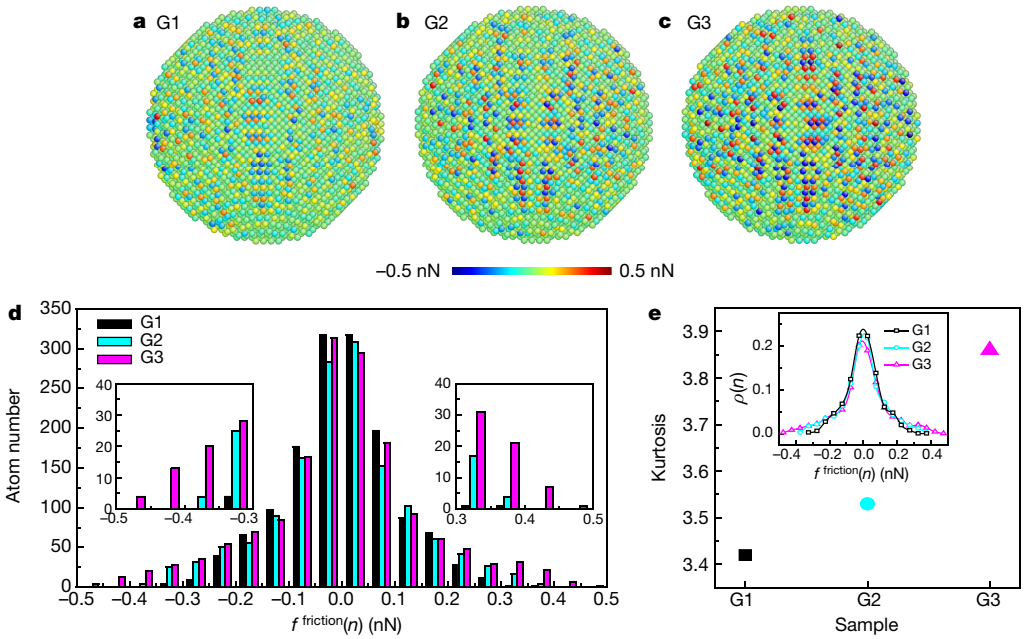


**Figure 4 | Evolution of the atomic-level forces contributing to friction on monolayer suspended graphene. a–c**, Comparison of $f_i^{\text{friction}}$ distribution in the three samples of Fig. 3b. **d**, The histograms of $f^{\text{friction}}(n)$ for the three samples. The insets provide a magnified view of the distribution in the tails. **e**, The kurtosis value of the distributions of $f^{\text{friction}}(n)$ for the three samples. The inset shows the force distributions that were used to calculate the kurtosis. $\rho(n)$ is the normalized atom number in each corresponding bin of interfacial forces.

indication that the tip–graphene interface became slightly more commensurate with each slip initially, and finally reached a stable value.

The simulations unambiguously show that the friction strengthening originates from two key mechanisms: enhancement of the local pinning (some individual atoms becoming more strongly pinned), and an increase in the interfacial commensurability (an increase in the number of atoms that are pinned in perfect synchrony). This is, to some extent, consistent with simulations of three-dimensional materials showing that interfacial commensurability, either through lattice matching[20] or through interaction-enhancing contaminant species, greatly increases static friction[21]. However, the evolution of interfacial friction and contact quality here is a result of high configurational freedom of graphene owing to its bending flexibility.

We then performed similar force analysis for multilayer ($N = 2$–4) graphene systems (see Supplementary Discussion 10) and found that the variation of the interfacial pinning and overall commensurability also contributed greatly to the layer dependence of friction, explaining the large quantitative disparity between the friction enhancement and true contact area increase in Fig. 1h. However, in the multilayer cases, the top graphene layer forms a perfect AB stacking with respect to the lower graphene layer. As observed in several experiments[2,22], perfectly aligned stacking can strongly constrain the relative lateral movement of graphene layers. This enhanced constraint reduces the ability of graphene to adjust its configuration during the sliding process.

Since the contact interface with graphene can be affected by pre-existing wrinkles[14], we speculate that regulating the degree of wrinkling[23] may offer an effective means of tuning friction. To test this, we studied a model system by sliding a tip over freely suspended graphene with various degrees of pre-existing wrinkling (Fig. 3a), formed by applying different amounts of bi-axial compressive strain ($\varepsilon_{xx}$ and $\varepsilon_{zz}$). Three samples G1, G2 and G3 with 0%, −0.2%, and −0.5% pre-compressive strain were studied in the simulations. As expected, the relaxation state of graphene profoundly affects its friction (Fig. 3b). Compared to G1, relaxed samples G2 and G3 exhibited substantially enhanced static friction (up to about 300%), although the increase in true contact area was much smaller (up to about 1.5%, see Fig. 3c). The $f_i^{\text{friction}}$ distributions at the local force peaks of these three samples (Fig. 4a–c) and their histograms (Fig. 4d) indicate that, as pre-compressive strain increased, stronger pinning sites with higher local interfacial forces appeared. Furthermore, the kurtosis analysis shows that the interfacial force distribution increasingly deviates from a unimodel Gaussian distribution from G1 to G3 (Fig. 4e), indicating a more commensurate interface with increasing pre-compressive strain.

As confirmed by the simulations, friction on suspended graphene can be effectively tuned by pre-compression and the 'quality' of the interfacial contact. But unlike the supported cases, the interface reached its steady configuration immediately after the tip made contact, because of larger excess area and resultant higher configurational flexibility. Thus, no frictional strengthening was observed in these simulations, consistent with the observations of Deng *et al.*[11]. We also performed simulations for graphene strongly bound to a flat surface. Owing to the much reduced freedom for graphene to configurationally evolve, no frictional strengthening or layer dependence occurred in this case either (see Supplementary Discussion 11), consistent with experimental measurements of strongly bound graphene[8,24].

In conclusion, we have identified a complementary aspect to the concept of true contact area governing friction on two-dimensional materials, related to evolving configurational relaxations that exploit out-of-plane floppiness. There is a general tendency for configurationally flexible systems to attain progressively deeper energy traps despite mechanical work being done to the system, improving the quality of contact. Imposing pre-compression on suspended graphene (to produce wrinkles) increased the total friction force several times with little change in the true contact area. This suggests a means of controlling friction of two-dimensional materials via strain engineering.

**Online Content** Methods, along with any additional Extended Data display items and Source Data, are available in the online version of the paper; references unique to these sections appear only in the online paper.

**Received 16 February; accepted 30 September 2016.**

1. Szlufarska, I., Chandross, M. & Carpick, R. W. Recent advances in single-asperity nanotribology. *J. Phys. D* **41,** 123001 (2008).
2. Dienwiebel, M. *et al.* Superlubricity of graphite. *Phys. Rev. Lett.* **92,** 126101 (2004).

3. Filippov, A. E., Dienwiebel, M., Frenken, J. W. M., Klafter, J. & Urbakh, M. Torque and twist against superlubricity. *Phys. Rev. Lett.* **100,** 046102 (2008).
4. Kim, W. K. & Falk, M. L. Atomic-scale simulations on the sliding of incommensurate surfaces: the breakdown of superlubricity. *Phys. Rev. B* **80,** 235428 (2009).
5. van Wijk, M., Dienwiebel, M., Frenken, J. & Fasolino, A. Superlubric to stick-slip sliding of incommensurate graphene flakes on graphite. *Phys. Rev. B* **88,** 235423 (2013).
6. Li, Q., Tullis, T. E., Goldsby, D. & Carpick, R. W. Frictional ageing from interfacial bonding and the origins of rate and state friction. *Nature* **480,** 233–236 (2011).
7. Liu, Y. & Szlufarska, I. Chemical origins of frictional aging. *Phys. Rev. Lett.* **109,** 186102 (2012).
8. Lee, C. *et al.* Frictional characteristics of atomically thin sheets. *Science* **328,** 76–80 (2010).
9. Chhowalla, M. & Amaratunga, G. A. Thin films of fullerene-like $MoS_2$ nanoparticles with ultralow friction and wear. *Nature* **407,** 164–167 (2000).
10. Choi, J. S. *et al.* Friction anisotropy-driven domain imaging on exfoliated monolayer graphene. *Science* **333,** 607–610 (2011).
11. Deng, Z. *et al.* Nanoscale interfacial friction and adhesion on supported versus suspended monolayer and multilayer graphene. *Langmuir* **29,** 235–243 (2013).
12. Cho, D.-H. *et al.* Effect of surface morphology on friction of graphene on various substrates. *Nanoscale* **5,** 3063–3069 (2013).
13. Filleter, T. *et al.* Friction and dissipation in epitaxial graphene films. *Phys. Rev. Lett.* **102,** 086102 (2009).
14. Ye, Z., Tang, C., Dong, Y. & Martini, A. Role of wrinkle height in friction variation with number of graphene layers. *J. Appl. Phys.* **112,** 116102 (2012).
15. Smolyanitsky, A., Killgore, J. & Tewary, V. Effect of elastic deformation on frictional properties of few-layer graphene. *Phys. Rev. B* **85,** 035412 (2012).
16. Ishigami, M., Chen, J. H., Cullen, W. G., Fuhrer, M. S. & Williams, E. D. Atomic structure of graphene on $SiO_2$. *Nano Lett.* **7,** 1643–1648 (2007).
17. Mate, C. M., McClelland, G. M., Erlandsson, R. & Chiang, S. Atomic-scale friction of a tungsten tip on a graphite surface. *Phys. Rev. Lett.* **59,** 1942–1945 (1987).
18. Bonelli, F., Manini, N., Cadelano, E. & Colombo, L. Atomistic simulations of the sliding friction of graphene flakes. *Eur. Phys. J. B* **70,** 449–459 (2009).
19. Li, Q., Lee, C., Carpick, R. W. & Hone, J. Substrate effect on thickness-dependent friction on graphene. *Phys. Stat. Sol. B* **247,** 2909–2914 (2010).
20. Luan, B. & Robbins, M. O. The breakdown of continuum models for mechanical contacts. *Nature* **435,** 929–932 (2005).
21. He, G., Müser, M. H. & Robbins, M. O. Adsorbed layers and the origin of static friction. *Science* **284,** 1650–1652 (1999).
22. Liu, Z. *et al.* Observation of microscale superlubricity in graphite. *Phys. Rev. Lett.* **108,** 205503 (2012).
23. Mohammadi, H. & Müser M. H. Friction of wrinkles. *Phys. Rev. Lett.* **105,** 224301 (2010).
24. Spear, J. C., Custer, J. P. & Batteas, J. D. The influence of nanoscale roughness and substrate chemistry on the frictional properties of single and few layer graphene. *Nanoscale* **7,** 10021–10029 (2015).


**Supplementary Information** is available in the online version of the paper.

**Acknowledgements** S.L. and P.G. appreciate support from the Alexander von Humboldt Foundation and the Helmholtz Programme Science and Technology of Nanosystems (STN). Q.L., X.D. and J.S. appreciate support from the 973 Programs of China (grant numbers 2013CB933003, 2013CB934201, 2015CB351903 and 2012CB619402), the NSFC (grant numbers 11422218, 11272177, 11432008, 51320105014 and 51321003), the International Joint Laboratory for Micro/Nano Manufacturing and Measurement Technologies, the Tsinghua University Initiative Scientific Research Program (grant number 2014Z01007), the Thousand Young Talents Program of China and 111 project (grant number B06025). R.W.C. acknowledges support from the NSF (grant numbers CMMI-1401164 and MRSEC DMR-1120901). J.L. acknowledges support from the NSF (grant numbers MRSEC DMR-1120901, CBET-1240696, DMR-1410636 and ECCS-1610806). We also thank J. Feng for discussions.

**Author Contributions** Q.L., R.W.C. and J.L. conceived and designed the project. S.L. performed molecular dynamics simulations. Q.L., R.W.C. and X.Z.L. provided information about the atomic force microscope experiments. Q.L., P.G., X.D., J.S. and J.L. provided the simulation guideline. S.L., Q.L., R.W.C. and J.L. wrote the paper. All authors contributed to discussions and analyses of the results.

**Author Information** Reprints and permissions information is available at www.nature.com/reprints. The authors declare no competing financial interests. Readers are welcome to comment on the online version of the paper. Correspondence and requests for materials should be addressed to Q.L. (qunyang@tsinghua.edu.cn), R.W.C. (carpick@seas.upenn.edu) or J.L. (liju@mit.edu).

## METHODS

**Atomistic simulations.** In the molecular dynamics simulations, we primarily studied the stick–slip friction of a tip sliding on two graphene systems: multilayer graphene supported on a rough amorphous silicon (a-Si) substrate; and suspended monolayer graphene. The covalent bonds of C–C in graphene[25] and Si–Si in amorphous substrate and in the crystalline Si tip[26] were described using the Tersoff and Stillinger–Weber potentials, respectively. A typical 6–12 Lennard–Jones potential was employed to describe van der Waals adhesive interaction between graphene and the substrate, graphene and the tip, and between the graphene layers. The Lennard–Jones parameters were chosen such that the work of adhesion ($E_{ad}$) or the pull-off force ($f_{ad}$) obtained by the molecular dynamics calculation were at the same scale as those from experimental measurements[11,16,27–29], as shown in Supplementary Table 1. The simulations were performed at 300 K using a Nosé–Hoover thermostat[30] with the LAMMPS[31] code. The atomic configurations are displayed using AtomEye[32].

For the graphene/a-Si substrate system, we first created an a-Si substrate by quenching liquid silicon from high temperature to 300 K using a cooling rate of $10^{13}$ K s$^{-1}$. The lateral dimension of the substrate was 43.4 nm × 43.4 nm ($x$–$z$ plane) with a thickness of approximately 3.0 nm. The atoms in the lowest 0.5 nm were held fixed. Owing to the free boundary condition along the out-of-plane ($y$) direction, roughness naturally formed on the free surface. A graphene sample, 38.5 nm × 38.6 nm in size was then placed above the a-Si within the adhesive interaction distance, and was then allowed to relax by approaching the substrate in response to adhesion. The root-mean-square roughness for the a-Si substrate and the relaxed graphene is 1.5 Å and 1.0 Å, respectively, close to experimental values[33]. After relaxation, a rigid ⟨001⟩-oriented crystalline silicon tip in a bowl-shape with a radius of 16.3 nm is placed in contact with the graphene.

The rigid tip assumption was based on the following considerations. First, previous experiments[8] have demonstrated that the layer-dependent friction on graphene was reproducible regardless of the tip material (that is, silicon, silicon nitride, or diamond). Second, using a rigid tip that is non-deformable makes it easier to trace the important yet subtle evolution of the interfacial forces.

To incorporate the compliance of atomic force microscope cantilever in experiments, we coupled harmonic springs in the $x$ direction for pulling the tip and in the $z$ direction for applying a fixed normal force. The stiffness of the normal springs is 30.0 N m$^{-1}$ and 0.16 N m$^{-1}$, comparable to the previous experiments[8]. The entire system was relaxed for 2 ns after adding the tip and further relaxed after the normal load was imposed. The friction tests were performed by displacing the lateral spring along $x$ direction with a constant velocity of 2 m s$^{-1}$ with a normal load of 0.8 nN applied, and calculating the lateral force acting on the virtual atom. To enhance the damping of oscillation (primarily along the lateral direction), we artificially decreased the tip mass by a factor of ten (see Supplementary Discussion 12). Simulations were performed at 300 K. Besides the rigid tip and the fixed atoms at the boundaries, all the other atoms in graphene and a-Si substrate were subjected to the thermostat. To further justify the rigid tip assumption, we carried out another simulation using a silicon tip sliding on monolayer graphene/a-Si substrate where all tip atoms were deformable but the topmost layer of atoms were rigid. We again obtained two-stage frictional behaviour (see Supplementary Discussion 13).

In the suspended graphene system, we created an ultraflat graphene sheet with dimensions of 38.5 nm × 38.6 nm in the $x$–$z$ plane. The boundaries were non-periodic. To constrain translational movement during tip sliding, the atoms near the boundaries were fixed rigidly. The tip was the same as that used in the supported system. We coupled a harmonic spring with a lateral stiffness of 30.0 N m$^{-1}$ and pulled the silicon tip at a velocity of 2 m s$^{-1}$ in the $x$ direction for friction tests. To minimize the boundary effects[14], a small sliding distance of 2.5 nm was used, compared to the much larger width of the graphene sheet (about 39 nm). Again, the simulations were carried out at 300 K.

**Contact area.** The contact area between the tip and graphene is estimated by setting a cutoff distance $r_c$ to judge whether graphene atoms are in intimate contact with the tip atoms. Here $r_c = 4$ Å, which is slightly larger than the equilibrium distance of the Lennard–Jones potential imposed on the tip–graphene interaction. The contact area is then obtained by multiplying the total number of attached graphene atoms by the graphene atomic area of 2.77 Å$^2$ per atom. It should be noted that the qualitative conclusions related to contact area are not affected even when we change the cutoff distance $r_c$ slightly. For example, the 20% increase of $r_c$ causes an increase of contact area by only 6%.

**Force analysis.** To minimize the influence of thermal fluctuation on interfacial forces, the force analyses were performed on quasistatic configurations which were obtained by further relaxing the system using the conjugate gradient method. This relaxation does not alter the frictional behaviour qualitatively, but it makes the statistical results more reliable and stable.

**Kurtosis.** The kurtosis is calculated as $K = \mu_4/\sigma^4$, where $\mu_4$ is the fourth moment about the mean value and $\sigma$ is the standard deviation of the distribution. Specifically, $\mu_4 = \sum_n (f^{\text{friction}}(n) - \overline{f})^4 \rho(n)$ and $\sigma^2 = \sum_n (f^{\text{friction}}(n) - \overline{f})^2 \rho(n)$, where $f^{\text{friction}}(n)$ is the atomic friction force of the $n$th bin, $\rho(n)$ is the normalized atom number in each corresponding bin and $\overline{f}$ is the mean value of $f^{\text{friction}}(n)$ of all bins, where $\overline{f} = \sum_n f^{\text{friction}}(n)\rho(n)$. In our case, kurtosis measures the 'peakedness' and 'tailedness' of the force distribution.

**Data availability.** The authors declare that all data supporting the findings of this study are available within the paper and its Supplementary Information.


25. Tersoff, J. Empirical interatomic potential for carbon, with applications to amorphous carbon. *Phys. Rev. Lett.* **61,** 2879–2882 (1988).
26. Stillinger, F. H. & Weber, T. A. Computer simulation of local order in condensed phases of silicon. *Phys. Rev. B* **31,** 5262–5271 (1985).
27. Zacharia, R., Ulbricht, H. & Hertel, T. Interlayer cohesive energy of graphite from thermal desorption of polyaromatic hydrocarbons. *Phys. Rev. B* **69,** 155406 (2004).
28. Zong, Z., Chen, C.-L., Dokmeci, M. R. & Wan, K.-t. Direct measurement of graphene adhesion on silicon surface by intercalation of nanoparticles. *J. Appl. Phys.* **107,** 026104 (2010).
29. Koenig, S. P., Boddeti, N. G., Dunn, M. L. & Bunch, J. S. Ultrastrong adhesion of graphene membranes. *Nat. Nanotechnol.* **6,** 543–546 (2011).
30. Nosé, S. A unified formulation of the constant temperature molecular-dynamics methods. *J. Chem. Phys.* **81,** 511–519 (1984).
31. Plimpton, S. Fast parallel algorithms for short-range molecular dynamics. *J. Comput. Phys.* **117,** 1–19 (1995).
32. Li, J. AtomEye: an efficient atomistic configuration viewer. *Model. Simul. Mater. Sci. Eng.* **11,** 173 (2003).
33. Giannazzo, F., Sonde, S., Nigro, R. L., Rimini, E. & Raineri, V. Mapping the density of scattering centers limiting the electron mean free path in graphene. *Nano Lett.* **11,** 4612–4618 (2011).

doi:10.1038/nature20135

**Supplementary Discussion 1 Morphology of multi-layer graphene in the presence of tip with a normal load of 0.8 nN and its influence on friction signal**

Figure 1 in the main text shows the morphology of monolayer graphene after the tip is placed in contact with it. Wrinkles are formed in the graphene, localized around the tip. We checked the morphology of multi-layer graphene to compare with the monolayer graphene system, as shown in Fig. S1. The left column shows the corresponding atomic configuration in a transverse view, where a vertical slice is cut through the center in order to view how the graphene sheet is deformed near the tip. We then extracted the top-view morphology of each layer, plotted to the right of each transverse view. We find that the layers in multi-layer graphene undergo some cooperative bending in the small area right beneath the tip. However, for the area around the edges of the tip-sample contact, only the top layer lifts off, partially wrapping around the tip. This separation is due to the competition between tip-graphene adhesion and interlayer adhesion among graphene sheets, resulting in out-of-plane deformation. In comparison to that of 2L, 3L and 4L graphene, the wrinkle height is largest in 1L graphene. The previous puckering model assumed that puckering was reduced because interlayer separation was negligible. This, thicker sheets were much more flexurally rigid. The simulations suggest that out-of-plane deformation, constrained to the topmost graphene layer, is a persistent feature and thus may occur even for bulk graphite samples. While the degree of out-of-plane deformation is layer-dependent, the dependence is modest. This suggests that additional mechanisms are contributing to the strong layer-dependent friction seen both in experiments and our simulations.

In order to know whether such layer separation could have a large influence on friction, we set up another friction test on multi-layer graphene where all layers lift off. Here we took the 2L graphene/a-Si substrate as an example to illustrate it. We made both layers lift off by keeping the tip-graphene interaction the same, but weakening the graphene-substrate interaction to be a half ($E_{ad}$ = 0.05 J/m$^2$) of that set in the manuscript ($E_{ad}$ = 0.1 J/m$^2$), as shown in Fig. S2a. The friction test was performed under the same condition as that in the manuscript. Figure S2b shows the lateral force as a function of distance. We found that the stick-slip motion follows almost the same two-stage friction trace, although the magnitude of friction drops a little bit in the constant force regime. The current simulations results confirm that frictional behavior is mostly governed by the interaction between tip and the topmost layer graphene.

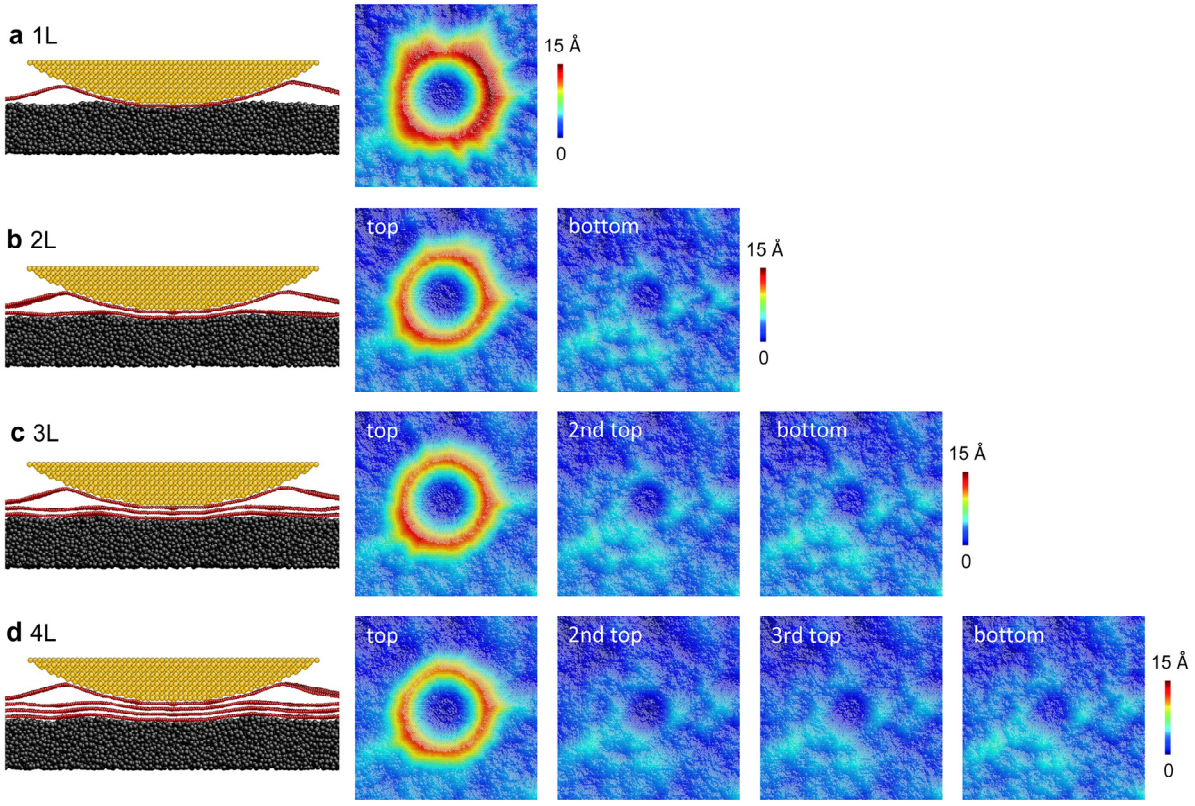


**Figure S1** The morphology of monolayer and multi-layer graphene in the presence of the tip. A normal load of 0.8 nN is applied. (a) 1L, (b) 2L, (c) 3L and (d) 4L graphene system. The leftmost image in each row is a cut-away view through the center of the tip, which reveals separation of the topmost layer around the edge of the tip-sample contact. The remaining images are top-views of each graphene layer. The color represents the corrugation height (the out-of-plane displacement of each graphene layer).

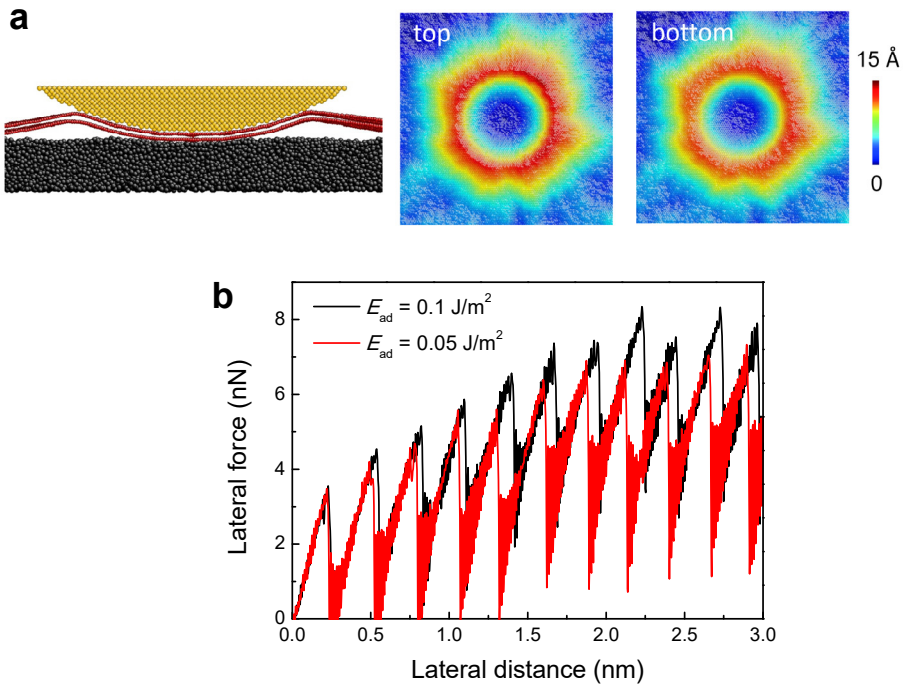


**Figure S2** Friction test on 2L graphene where both layers lifts off. (a) The simulation model. The adhesion energy of graphene-substrate is weakened to make both graphene layers life off upon the adhesion by the tip. (b) Friction signal of stick-slip motion in comparison to that in manuscript where only the topmost layer lifts off.

**Supplementary Discussion 2 Variation of normal load in friction simulation**

In the graphene/a-Si substrate system, the normal spring constant we chose in the simulation, 0.16 N/m, was based on values used in the corresponding experiments. In those experiments, multiple probes were used and the normal spring constants were typically in the range of 0.1~0.2 N/m (see ref. 7). We paid special attention to ensure that the normal force in our simulations remained stable. Figure S3 shows a typical variation of normal force during a sliding simulation with layer numbers $N$ = 1-4.

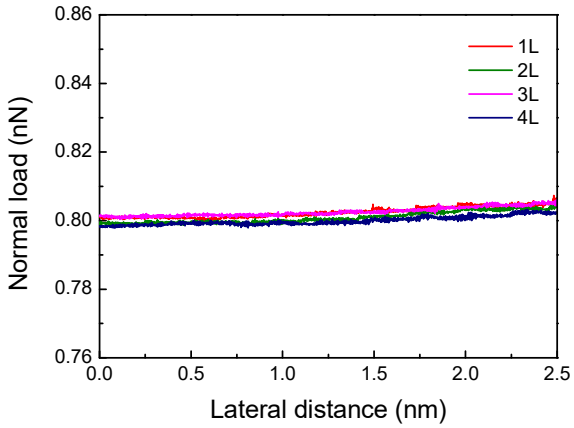


**Figure S3** Typical variation of normal load as a function of lateral distance in graphene/a-Si substrate.

**Supplementary Discussion 3 The effect of sliding speed on friction in the 1L graphene/a-Si substrate system**

In MD simulations, we used a pulling velocity of 2 m/s to drag the tip, which is several orders of magnitude larger than that in experiments. Despite the drastically different time scales, previous studies have shown that MD simulations can offer unique and valuable atomic-scale information about sliding interfaces, especially when energetics are concerned[8-10]. We took careful attentions to ensure the simulation results obtained do not arise from artifacts due to the different kinetics. To address this issue, we performed further simulations to confirm that our results do not come from non-equilibrated high-speed pulling. We first performed another two sets of simulation by reducing the sliding speed from 2 m/s down to 1 m/s and 0.5 m/s. As shown in Fig. S4, the friction force traces with reduced sliding speeds are very similar to the original case, with apparent two-stage strengthening behavior. Although we could not reduce the sliding speed to a much lower value due to the constraint of the computational cost, the weak dependence of the friction strengthening behavior on sliding speed suggests that the evolution of the interface is less likely to be erroneously caused by the high pulling speed.

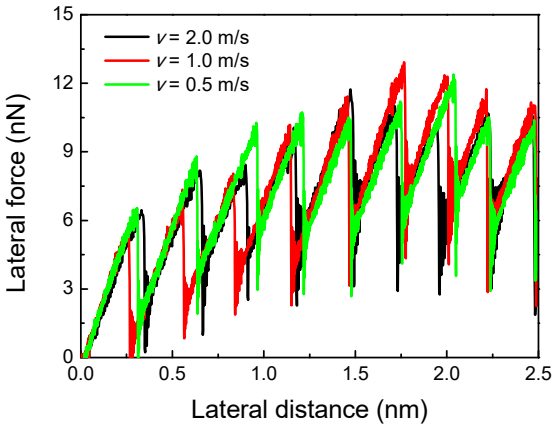


**Figure S4** The lateral force *vs.* lateral distance, under different pulling speeds.

**Supplementary Discussion 4 The quasi-static calculation of stick-slip motion in the 1L graphene/a-Si substrate system**

To further confirm that the two-stage friction was not a dynamic effect caused by the high sliding speed, we used a quasi-static approach[11,12] to perform the friction test for the 1L graphene/a-Si substrate system. This method essentially excludes the temperature and dynamic effects. Specifically, the tip atoms are coupled horizontally to a rigid "support" by a linear spring with a spring constant of 0.003 N/m. Then we moved the support laterally step-by-step at an interval of 0.2 Å. For each step, we used conjugate gradient techniques to relax the system. The lateral force was calculated by sum up the force on each tip atom. Figure S5 shows the trace of the lateral force vs. lateral distance obtained from this quasi-static simulation. Once again, a similar two-stage friction was reproduced for the 1L graphene/a-Si substrate, *i.e.* the friction first underwent strengthening and then entered a stage of nearly steady peak friction force. In comparison to the simulation results at 300 K, the local peak lateral force oscillated moderately. As revealed in our simulations, friction variation is dependent on the evolution of graphene, which relies on its interaction with both tip and the deformed substrate. The detailed deformation process of individual atoms of the amorphous-phase Si during the quasi-static simulation (corresponding to 0 K) can be slightly different from that at 300 K. The difference of such deformation ability might affect the evolution of graphene and influence the friction force signal. Nevertheless, the friction strengthening effect was clearly preserved. This confirms that our previous observations and conclusions are not artifacts due to the high sliding speed in our simulations.

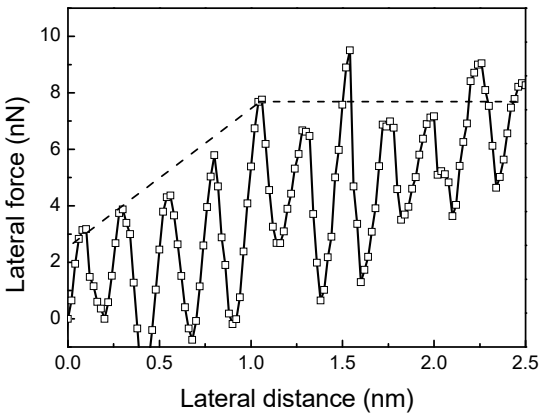


**Figure S5** Friction signal obtained by quasi-static calculations in 1L graphene/a-Si substrate.

**Supplementary Discussion 5 Calculation of the energy barrier for one stick-slip event**

The issue of timescale is indeed key when comparing atomistic simulations with experiments[13,14]. Importantly, recent MD simulations and AFM experiments of atomic-scale friction with close and even matching sliding speeds showed that sliding mechanisms and energetic parameters matched well between the two; a discrepancy in force values could be accounted for by simply considering the smaller mass (and higher vibration frequencies) in the simulations[8,9]. Collectively, this gives some confidence to the reliability of using MD for understanding AFM experimental results.

However, to establish further reliability, one can evaluate the energy barrier. This is a good way to check whether the observed behavior is an artifact of the relatively high-speed simulations. In particular, it helps us estimate the time scale at which a spontaneous slip motion can be driven by thermal activation. In atomistic simulations, the climbed image nudged elastic band (CINEB) method[15,16] is widely used method to search for the minimum energy pathway and the corresponding activation barrier. Therefore, we used this method to calculate the barriers in the first stick-slip cycle for both suspended graphene (G1 sample in Fig. 3a of manuscript) and for the a-Si supported graphene (1L graphene/a-Si sample). Figure S6a shows that the energy pathway of the suspended graphene has an energy barrier of approximately 1.8 eV. Because the initial and final configurations are nearly equivalent, they stay in almost the same energy states. The activation pathway in the first stick-slip event of 1L graphene/a-Si substrate system is given in Fig. S6b. The activation energy barrier is again quite significant (approximately 4 eV). We note that, in contrast to the suspended case, the energy in the final state in the supported case is higher than that in initial state. The increase of energy arises primarily from elastic deformation of the a-Si substrate as well as the configuration of the evolved graphene as the tip slides forward.

With the energy barriers above, we can then estimate whether the thermal activation could have a significant effect on the stick-slip motion or not. The scan speed ($v$) in AFM experiments is typically on the order of 1~10 nm/s. For the stick-slip motion on graphene, the slip distance ($d$) is roughly the period of one hexagonal carbon lattice (0.25 nm). Now the thermal-activated threshold barrier ($\Delta E_{th}$) that the tip needs to overcome can be estimated as $v/d = \upsilon_0 \exp(-\Delta E_{th}/k_B T)$, where $\upsilon_0$ is the attempt frequency at high-speed limit, $k_B$ is Boltzmann constant and $T$ is absolute temperature. The magnitude of $\upsilon_0$ is on the order of $10^{10}$ $s^{-1}$ because of the relatively large

effective mass associated with the stick-slip motion in comparison to a single atom or molecule. It includes all tip atoms in the simulations, and it may even include the whole cantilever for real experiments (see more in ref. 8). The $\Delta E_{th}$ is obtained to be around 0.56 eV with $v$ = 1 nm/s at $T$ = 300 K, much smaller than the real barrier we obtained above. Therefore, even if our simulations were carried out with a realistic low speed, the thermal activation is still unlikely to play an important role.

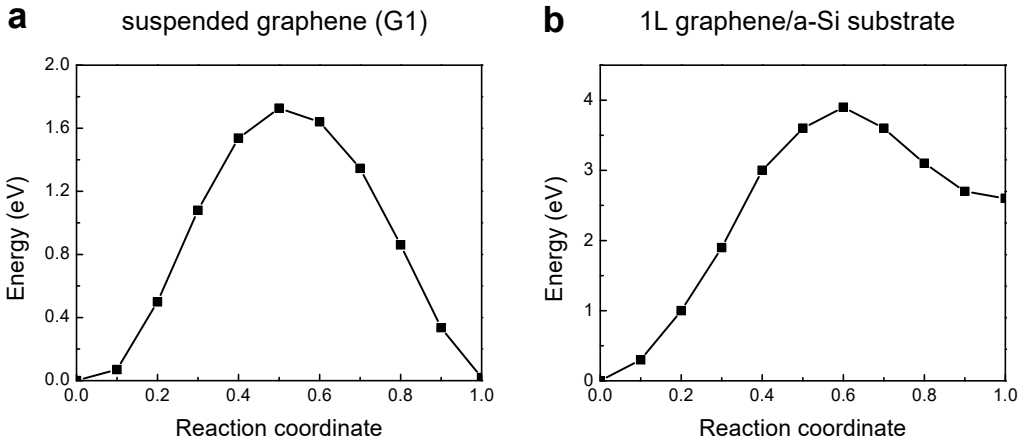


**Figure S6** The activation pathways in the first stick-slip motion of (a) suspended graphene (sample G1) and (b) 1L graphene/a-Si substrate calculated using the CINEB method.

**Supplementary Discussion 6 The distribution of $f_i(0)$ and $f_i^{\text{Friction}}$ in tip**

As mentioned in the main text, there already exists a locally non-zero but globally self-equilibrated distribution of tip-graphene interfacial forces even before sliding. Figure S7 shows the distribution of $x$-component of this interaction force at $x_{\text{spr}} = 0$ as $f_i(0)$ in the monolayer graphene/a-Si substrate system.

We further checked the distribution of $f_i^{\text{Friction}}$ in tip and found that the forces are mostly undertaken by the outer and second outer surfaces of tip. Figure S8 shows a snapshot of tip when sliding on the graphene/a-Si substrate system (the applied force from the spring is to the right). The colors in Fig. S8a and Fig. S8b are displayed by atomic friction force ($f_i^{\text{Friction}}$) and coordination number (CN), respective. We then cut the tip to examine the atomic friction force in the core region of tip, as shown in Fig. S8c-d. We find that, besides the outer surface (CN = 2) and second outer surface (CN = 3), the tip atoms in the inner layer contribute little to the friction.

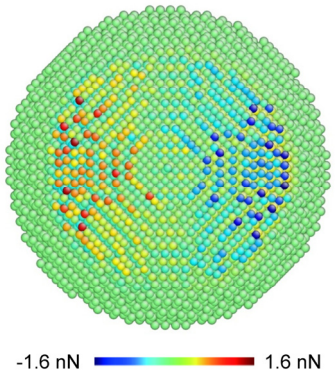


**Figure S7** The distribution of the $x$-component of the tip-graphene interaction force at $x_{\text{spr}} = 0$ in the monolayer graphene/a-Si substrate system. The positive force direction (yellow to red) is to the right.

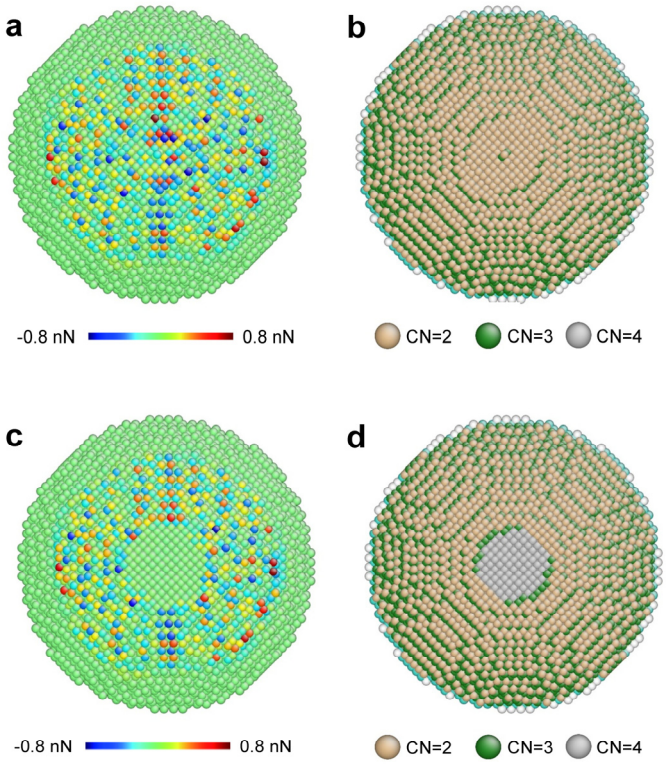


**Figure S8** (a)-(b) A snapshot of the tip configuration while being pulled to the right. (c)-(d) The tip is further cut to show the core region. The images are colored according to $f_i^{\text{Friction}}$ distribution in (a), (c), and according to coordination number (CN) in (b), (d). The positive force direction (yellow to red) is to the right.

**Supplementary Discussion 7 The $f_i^{\text{Friction}}$ trace of individual tip atoms during tip sliding in graphene/a-Si substrate**

To understand better how the local pinning sites affect the resistance to sliding, we followed the trace of $f_i^{\text{Friction}}$ of the individual tip atoms during sliding for the monolayer graphene/a-Si substrate system. As mentioned in the previous section, the atomic friction forces are primarily sustained by the tip atoms on the outer surface. We thus chose all the surface atoms (CN = 2) and individually followed their force traces during sliding (Fig. S9a). The total amount of surface atoms that are taken into account is approximately 800. We know the atoms with negative values of $f_i^{\text{Friction}}$ will act as the pinning sites, and those with positive values will act as pushing sites. Here we only focus on the pinning sites. We found that, among all the atoms, only a few atoms exhibit the two-stage friction behavior (where there is a transient strengthening stage, followed by a stage of constant static friction, *i.e.*, where the force at which the tip slips in each stick-slip cycle remains constant) (Fig. S9b), which corresponds to the two-stage friction measured by the spring. The majority of the atoms show a constant static friction force, as shown by representative traces in Fig. S9c.

As we stated in the main text, the variation of interfacial force is closely related to the local configuration of the contacting graphene. To show this, we examined the nearby graphene atomic configuration around individual tip atom (within a radius of 1 nm). Figure S10 shows the atomic configuration of nearby graphene for tip atoms #1 and #8 at different friction states, which correspond to the original state and the following i~iv states in Fig. 1g of the main text. For tip atom #1, whose interfacial force exhibited two-stage variation, the nearby graphene configuration changed during the strengthening stage, but became stable during the steady state. However, for tip atom #8 whose interfacial force underwent normal stick-slip variation, the local configuration of nearby graphene was almost unchanged. The reason why tip atoms #1, #2, #3, #4 play a special role in the interfacial force evolution is that their nearby environment allows certain room for the floppy graphene to adjust its atomic configuration and increase the resulting local pinning forces.

Furthermore, since this is occurring under a sliding tip, the strengthening process is dynamically induced by the sliding itself; the new graphene atoms that are brought into the contact zone via shear displacement are able to find more traps and trap more deeply. This is consistent with the finding that adhesion (measured via pull-off forces) is higher when a tip is slid against graphene just prior to pull-off as compared to adhesion measured by approaching and then retracting the tip with no sliding during the contact[17].

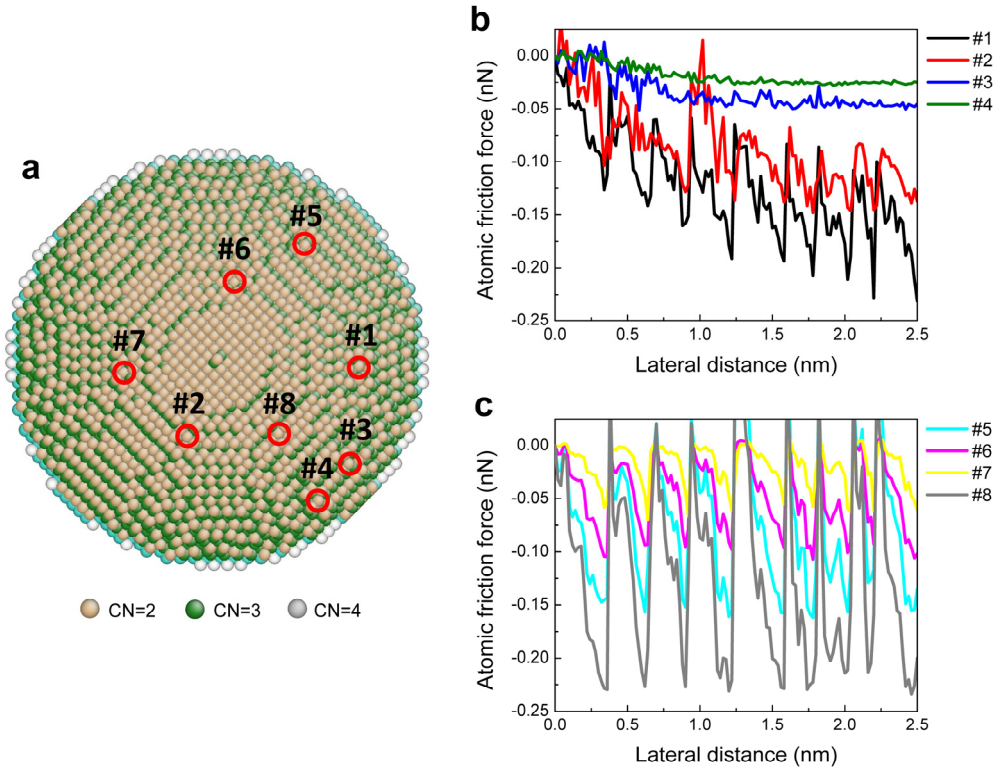


**Figure S9** The $f_i^{\text{Friction}}$ traces of individual atoms at the surface of the tip during sliding for the graphene/a-Si substrate system. (a) Specific atoms on the outer surface of the tip are indicated. The various force traces in (b) show cases that exhibit two-stage friction (strengthening followed by constant static friction) while the force traces shown in (c) exhibit constant static friction.

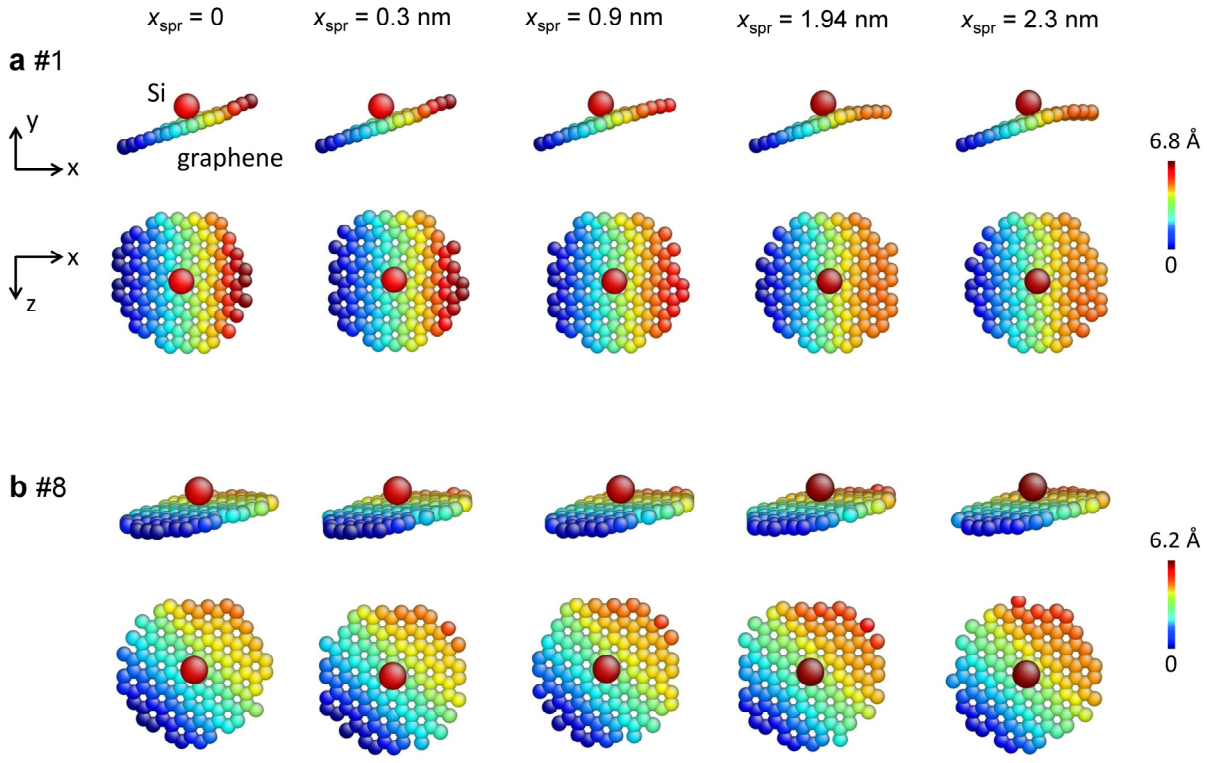


**Figure S10** Snapshot of individual tip atoms and the atomic configurations of nearby graphene during sliding for (a) atom #1 and (b) atom #8 in the tip. The force on tip atom #1 exhibits two-stage variation and the force on tip atom #8 undergoes regular stick-slip variation.

**Supplementary Discussion 8 Evolution of graphene configuration for 1L and 4L graphene/a-Si substrate**

We examined the evolution of the graphene film's configuration during sliding for the graphene/a-Si substrate system. Figure S11a shows stick-slip motion on 1L graphene with several specific points selected. Figures S11b-f show the corresponding atomic images marked in Fig. S11a. The top row shows the side view of both tip and graphene configurations and the bottom row shows the top view of the graphene only. To amplify the local configuration, we do not show all of the graphene, but only a small localized region beneath tip within a height of 4 Å. Here, the height is measured by taking the lowest point of the graphene (beneath the center of the tip) for each snapshot as the reference. From the images, we observe a change in the configuration of the graphene from the point o to point iii in the strengthening stage evident by the change in contrast and diameter of the plotted region seen in the top view, but very little change between points iii and iv, in the constant slip force constant regime. This indicates the variation of local curvature of graphene as the schematic illustration shown in Fig. S11g, where the overall curvature increases during the strengthening stage, indicating increased geometric conformality with the tip. For comparison, we also did the similar analysis to 4L graphene, as shown in Fig. S12. In contrast to the results for 1L graphene, the configuration of the 4L graphene does not undergo an obvious evolution. This is consistent with the much smaller strengthening effect and the reduced friction in the constant slip force regime. Note that there was no atomic bond breaking or rehybridization observed in graphene during sliding, which implied that the deformation of graphene was always in the elastic and non-wear regime.

Although this morphology evolution (or lack thereof) correlates with the change in commensurability, we still should be careful in making any direct linkage between the two because the accurate characteristic of interface commensurability at atomic scale requires a three-dimensional view.

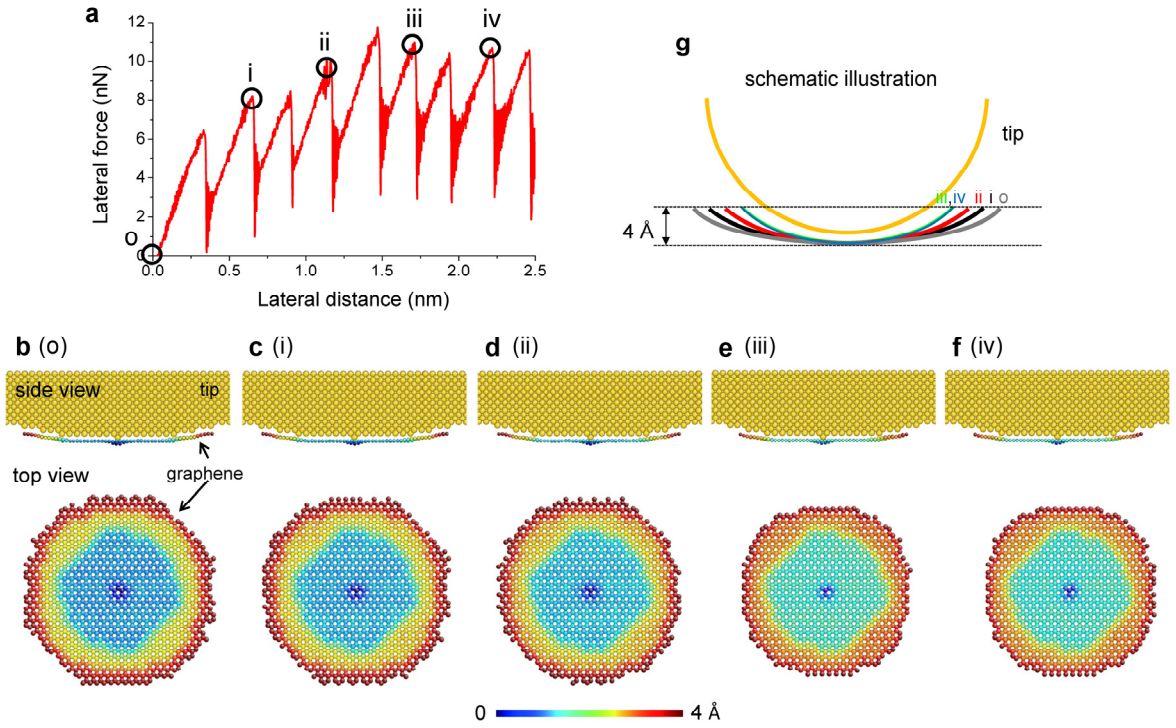


**Figure S11** The graphene configuration during sliding for the 1L graphene/a-Si substrate system. (a) The lateral force trace with several typical points indicated. (b)-(f) The corresponding atomic images for the points indicated in (a). The top and bottom rows are viewed from the side and top, respectively. The graphene atoms are colored according to their height. (g) Schematic illustration.

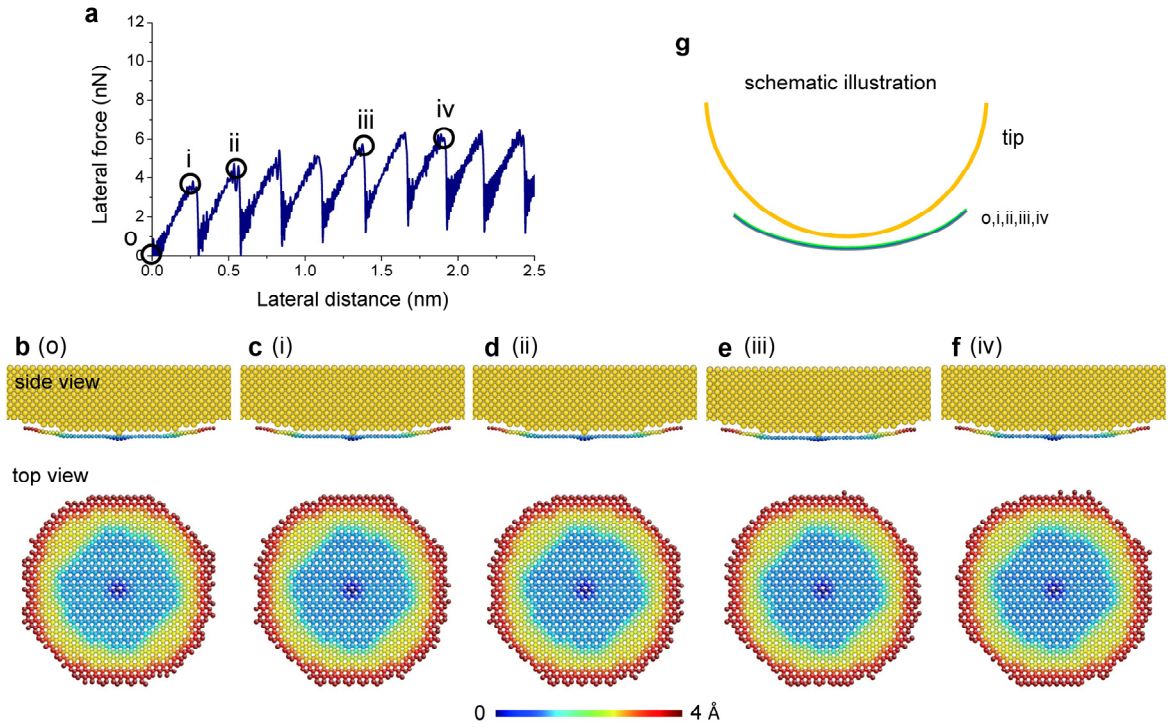


**Figure S12** The graphene configuration during sliding in 4L graphene/a-Si substrate system. (a) The lateral force trace. (b)-(f) The corresponding atomic images indicated in (a). (g) Schematic illustration.

**Supplementary Discussion 9 Interpretation of kurtosis**

In the main text, we analyzed the distribution of atomic friction forces in terms of kurtosis. Figure S13 shows several typical unimodal distributions and their excess kurtosis value (≡ kurtosis - 3), with their variance, $\sigma^2$, constrained to be constant. A Gaussian distribution has a kurtosis value of 3. A uniform distribution has a kurtosis value of 1.8. The uniform and Gaussian distributions are representative of unimodal distributions, which is the outcome of structureless randomness. Distributions with long tails (tailedness) and compensating tall peak (peakedness) have kurtosis values larger than the Gaussian or uniform distributions, and they typically are manifestations of more structured interfaces. An example of such high-kurtosis distribution would be the superposition of two Gaussians, one with a narrower $\sigma_1^2$ and the other with a wider $\sigma_2^2$, with fixed $\sigma^2 = w_1\sigma_1^2 + w_2\sigma_2^2$ where $w_1$ and $w_2$ are the mixing weights of the first and second Gaussian respectively. Such a distribution would represent a bipartite atomic population, one with smaller force fluctuations, and one with larger force fluctuations.

Our force distribution profile of $f_i^{\,friction}$ shows noticeable increases in the peakedness and tailedness as the system reaches points iii and iv (Fig. 2c and 2d in the main text), with kurtosis close to 5.5. Such a larger kurtosis and deviation from a Gaussian distribution indicate an underlying structure that drives the distribution away from unimodality. When viewing the spatial distribution of forces in Fig. 2c or 2d, one can see a double-periodicity along the *z* direction, i.e. the forces are strongly alternating along *z* direction at a given instant. In contrast, the force exhibits strong single-atom periodicity along the *x* direction, *i.e.*, at a given instant, the forces on the tip atoms are often of the same sign and similar magnitude for a few atoms in a row along the *x* direction. This is illustrated in Fig. S14.

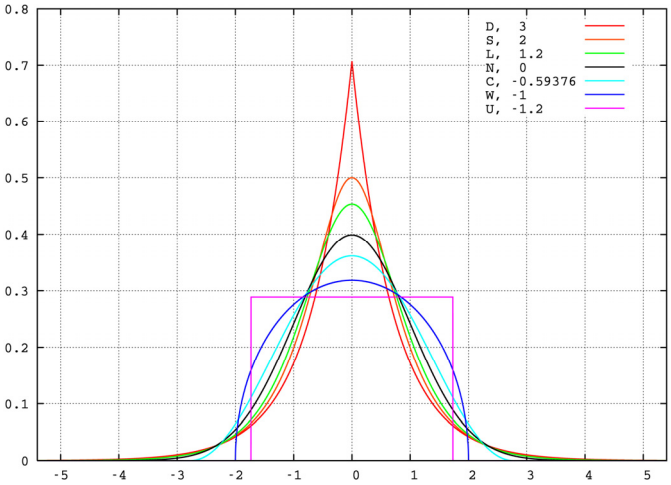


**Figure S13** Kurtosis in different distributions. Here the values in the figure refer to the excess kurtosis, which is the kurtosis minus 3.0. More details can be found in Wikipedia (https://en.wikipedia.org/wiki/Kurtosis)

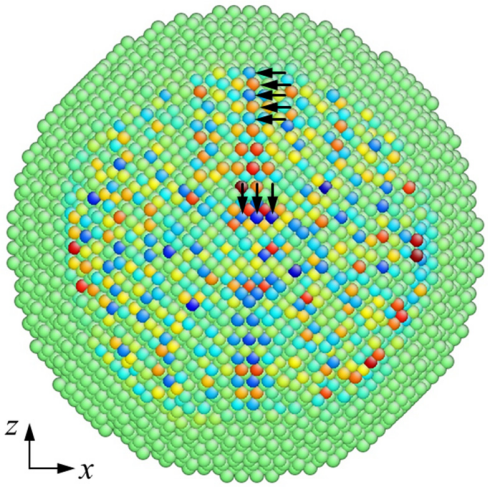


**Figure S14** The periodicity of force distribution. The horizontal and vertical arrows indicate the double-periodicity along *z* direction and single periodicity along *x* direction, respectively.

**Supplementary Discussion 10 Force analysis in multi-layer graphene ($N$ = 2~4)**

We selected several points where the lateral force reaches a maximum (*i.e.* the static friction force) during stick-slip sliding to show the friction force distribution ($f_i^{\text{Friction}}$) during friction in multi-layer graphene samples ($N$ = 2~4), as shown in Figs S15a-c. Similar to that in monolayer graphene, the density and strength of pinning points go up in the strengthening stage, and become almost unchanged in the constant friction force stage. Comparing the magnitude of static friction force for different numbers of layers of graphene, we can roughly see that the magnitude becomes smaller as layer number increases. The force analysis in multi-layer graphene further confirms that the friction in graphene thin sheets is governed by the interfacial pinning and commensurability.

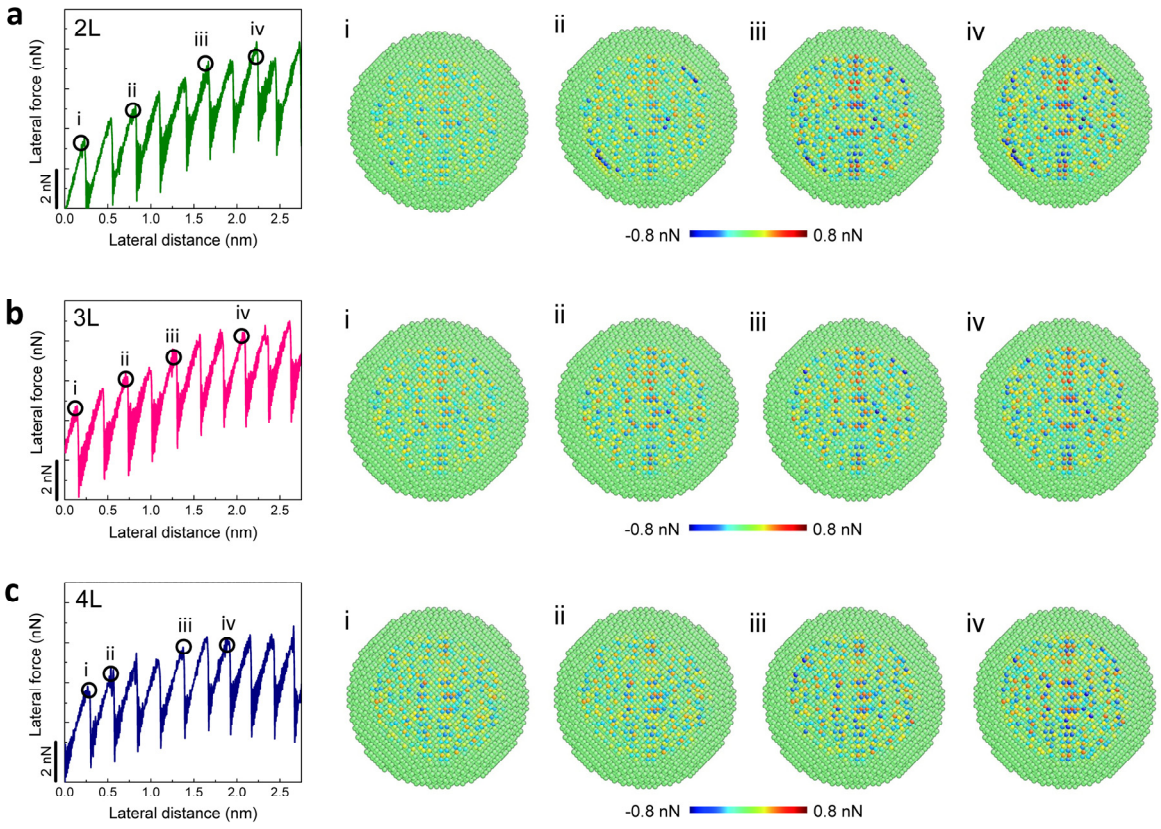


**Figure S15** Evolution of the atomic friction force ($f_i^{\text{Friction}}$) during sliding in multi-layer graphene for (a) 2L, (b) 3L, and (c) 4L samples.

**Supplementary Discussion 11 Friction for the graphene/mica substrate**

Previous experiments showed that the layer-dependent friction effect was suppressed if the graphene is adhered to a highly adhesive substrate (muscovite mica)[7]. To simulate the friction for a tip sliding on graphene supported by mica, we constructed a simple "effective mica" model by placing graphene on an ultra-flat surface that with an extremely large stiffness and high adhesion with graphene. Figures S16a and S16b show the model of 1L and 2L graphene placed on this effective mica substrate. The interaction between graphene and the substrate is modeled by a 6-12 type LJ potential as before, but as shown in Supplementary Table 1, the parameters were set to be $\varepsilon = 0.023$ eV (2.4 times larger than the value of 0.0096 used for the a-Si substrate) and $\sigma =$ 3.0 Å, which results in an adhesion energy between graphene and substrate of 114.8 meV per carbon atom (corresponding to 0.66 J/m$^2$), close to that by density functional theory (DFT) calculations[6] and much higher than the graphene-a-Si experimental range of 0.1-0.45 J/m$^2$. The tip was the same as that used in the manuscript. The friction tests were performed with a normal load of 0.8 nN applied. Figure S16c shows the lateral spring force as a function of distance in a 3 nm scan trace at 300 K. In contrast with the graphene/a-Si substrate, there is no strengthening stage or obvious layer-dependent behaviors, which qualitatively agree with the experimental observations[7].

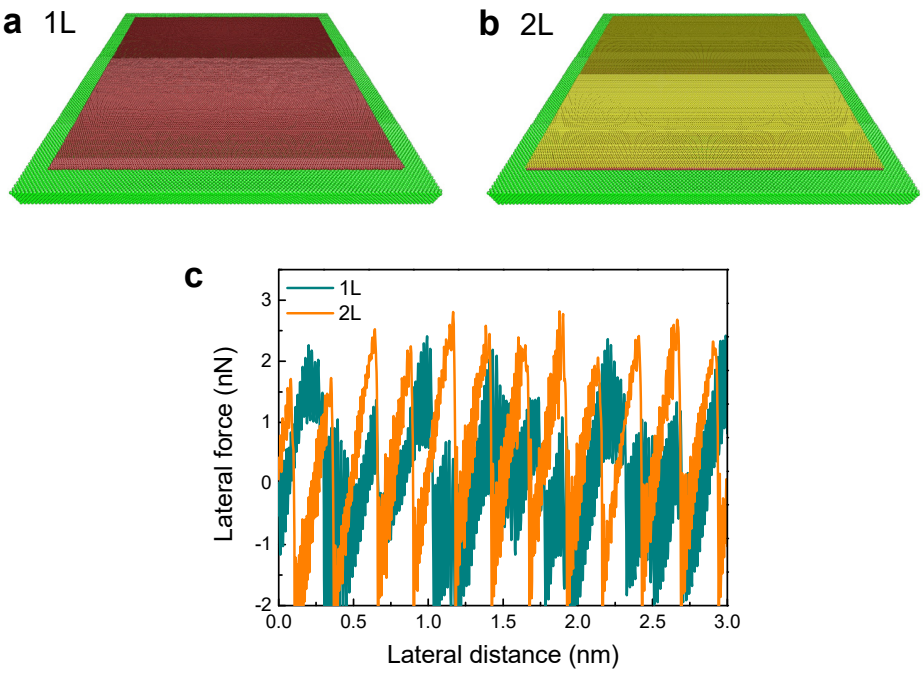


**Figure S16** Stick-slip motion on graphene/mica system. (a)-(b) Simulation model for 1L and 2L graphene. (c) Lateral spring force trace of two samples.

**Supplementary Discussion 12 Enhancement of damping by artificially reducing tip mass**

In the MD simulations, the kinetic energy of the sliding tip after a local slip is dissipated through graphene and the supporting substrate by a thermostat. Direct damping to the spring is typically not used to avoid unphysical interference to the slip process. Because of this configuration, after the tip jumps in one stick-slip event, the tip can have a large instantaneous slip speed, and can oscillate in the next cycle if the damping is not strong enough. This is shown in the red friction force curve in Fig. S17 when the real tip mass ($m = m_0$) is used for the 1L graphene/a-Si substrate system. To damp out the oscillation more efficiently, we artificially reduced the mass of the tip atoms, therefore the kinetic energy could be damped more quickly, giving a smoother force curve (the black curve in Fig. S17). As indicated by the two curves in Fig. S17, simulations with this artificial treatment produced quantitatively similar results as the original one. This is understandable since our simulations were good approximation for quasistatic sliding as we have demonstrated in Supplementary Discussion 4.

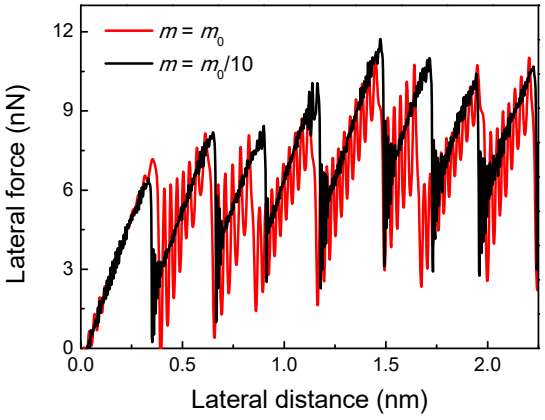


**Figure S17** Comparison of the lateral force signal obtained by changing tip mass in 1L graphene/a-Si substrate. Black and red traces refer to the original mass ($m = m_0$) and the mass reduced by a factor of 10 respectively.

**Supplementary Discussion 13 Friction in 1L graphene/a-Si substrate by using a deformable silicon tip**

In the main text, we used a rigid tip that is non-deformable for the friction simulation in order to show the important but subtle evolution of the interfacial forces clearly. To exclude the possible influence of using a rigid tip on the results, we carried out another simulation by using a deformable <001>-oriented crystalline silicon tip sliding on 1L graphene/a-Si substrate, as indicated in Fig. S18a. In this new simulation, only the top few layers of the Si tip were fixed (yellow color, 14566 atoms) and all the remaining atoms (dark red color, 1884 atoms) were fully free. In the sliding simulation, the spring pulling force was applied to the fixed layers to drive the tip to move at the same velocity as before (2 m/s). To save computational time, we used a smaller tip with the radius of 5.4 nm (leaving the tip the same size would have required a few weeks of computation despite using state-of-the-art algorithms and parallel computing resources). We also re-adjusted the LJ parameters of tip-graphene interaction to make sure the effective work of adhesion is at the same level as before. Figure S18b shows the resulting lateral force trace with lateral distance in the new simulations. Because of the smaller tip used, the final steady-state friction force was lower than the previous cases, which is expected (e.g., see the size dependence found in ref. 9). Although the friction forces and slip distances in the steady-state stage oscillated slightly (likely due to the randomly rough substrate and the extra deformation capability of the Si tip), the two-stage friction with an initial strengthening was very clear and reproducible. Therefore, we believe that the behavior we observed previously is not sensitive to the deformability of the tip.

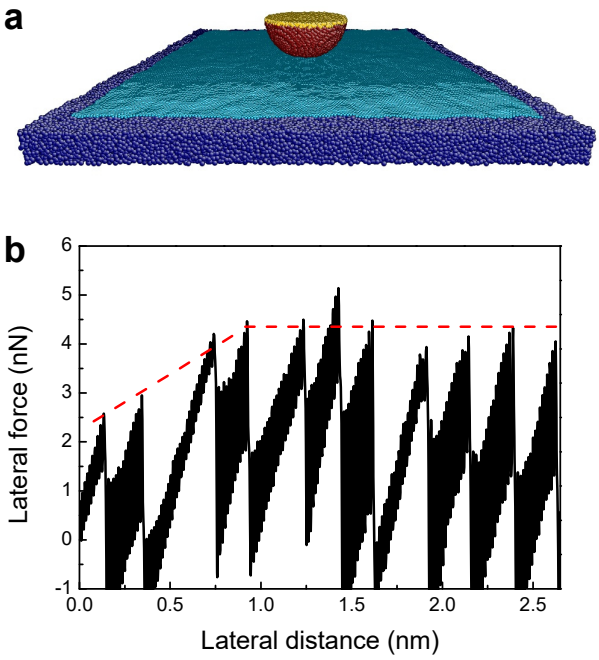


**Figure S18** Lateral force for a free crystalline silicon tip sliding on 1L graphene/a-Si substrate. (a) Simulation model. The atoms in dark blue and light blue refer to the a-Si substrate and graphene. The atoms in yellow are fixed layers in tip and all the other atoms in dark red are free. (b) The lateral force vs lateral distance. The two-stage stick-slip motion is clearly observed.

| van der Waals interactions | $\varepsilon$ (eV) | $\sigma$ (Å) | $E_{ad}$ ($J/m^2$) | | $f_{ad}$ (nN) | |
|---|---|---|---|---|---|---|
| graphene —silicon tip | 0.092 | 3.0 | — | — | 7.7 for $r_{tip}$ = 8.0 nm (ref. 1) | 47.3 for $r_{tip}$ = 16.3 nm (present) |
| graphene —graphene | 0.0024 | 3.4 | 0.03 (ref. 2) | 0.03 (present) | — | — |
| graphene —a-Si substrate | 0.0096 | 3.0 | 0.1-0.45 (refs 3-5) | 0.1 (present) | — | — |
| graphene —effective mica substrate | 0.023 | 3.0 | 0.66 (ref. 6) | 0.66 (present) | — | — |

**Supplementary Table 1 Parameters of the 6-12 Lennard-Jones potential for the different types of van der Waals interactions used in the simulations.** The $\varepsilon$ and $\sigma$ parameters are in units of eV and Å, respectively. The calculated adhesion energy $E_{ad}$ and adhesion force $f_{ad}$ are in units of $J/m^2$ and nN, respectively. The value of $E_{ad}$ and $f_{ad}$ calculated from MD simulations are also compared with values from experimental measurements. The adhesion energy between monolayer graphene and the $SiO_2$ substrate ranges from 0.1-0.45 $J/m^2$ as obtained by different groups, and our simulations gave a value of 0.1 $J/m^2$. The adhesion energy between graphene-graphene interlayers is set to be 0.03 $J/m^2$, the same as that in bulk graphite. The adhesion force between tip and graphene should be proportional to tip radius ($r_{tip}$), according to continuum contact mechanics theories. The value of $f_{ad}$ is measured to be 7.7 nN at $r_{tip}$ = 8.0 nm in experiments. Our simulation used a larger tip and set $f_{ad}$ to be 47.3 nN at $r_{tip}$ = 16.3 nm. Values are also included for the effective mica substrate discussed below in Supplementary Discussion 11.

## References for Supplementary Information


1 Deng, Z. *et al.* Nanoscale interfacial friction and adhesion on supported versus suspended monolayer and multilayer graphene. *Langmuir* **29**, 235-243 (2013).

2 Zacharia, R., Ulbricht, H. & Hertel, T. Interlayer cohesive energy of graphite from thermal desorption of polyaromatic hydrocarbons. *Phys. Rev. B* **69**, 155406 (2004).

3 Ishigami, M., Chen, J. H., Cullen, W. G., Fuhrer, M. S. & Williams, E. D. Atomic structure of graphene on $SiO_2$. *Nano Lett.* **7**, 1643-1648 (2007).

4 Zong, Z., Chen, C.-L., Dokmeci, M. R. & Wan, K.-t. Direct measurement of graphene adhesion on silicon surface by intercalation of nanoparticles. *J. Appl. Phys.* **107**, 026104 (2010).

5 Koenig, S. P., Boddeti, N. G., Dunn, M. L. & Bunch, J. S. Ultrastrong adhesion of graphene membranes. *Nature Nanotechnol.* **6**, 543-546 (2011).

6 Rudenko, A., Keil, F., Katsnelson, M. & Lichtenstein, A. Graphene adhesion on mica: Role of surface morphology. *Phys. Rev. B* **83**, 045409 (2011).

7 Lee, C. *et al.* Frictional characteristics of atomically thin sheets. *Science* **328**, 76-80 (2010).

8 Li, Q., Dong, Y., Perez, D., Martini, A. & Carpick, R. W. Speed dependence of atomic stick-slip friction in optimally matched experiments and molecular dynamics simulations. *Phys. Rev. Lett.* **106**, 126101 (2011).

9 Liu, X.-Z. *et al.* Dynamics of atomic stick-slip friction examined with atomic force microscopy and atomistic simulations at overlapping speeds. *Phys. Rev. Lett.* **114**, 146102 (2015).

10 Szlufarska, I., Chandross, M. & Carpick, R. W. Recent advances in single-asperity nanotribology. *J. Phys. D* **41**, 123001 (2008).

11 Bonelli, F., Manini, N., Cadelano, E. & Colombo, L. Atomistic simulations of the sliding friction of graphene flakes. *Eur. Phys. J. B* **70**, 449-459 (2009).

12 Van Wijk, M., Dienwiebel, M., Frenken, J. & Fasolino, A. Superlubric to stick-slip sliding of incommensurate graphene flakes on graphite. *Phys. Rev. B* **88**, 235423 (2013).

13 Zhu, T., Li, J., Samanta, A., Leach, A. & Gall, K. Temperature and strain-rate dependence of surface dislocation nucleation. *Phys. Rev. Lett.* **100**, 025502 (2008).

14 Li, J. The mechanics and physics of defect nucleation. *MRS Bull.* **32**, 151-159 (2007).

15 Henkelman, G., Uberuaga, B. P. & Jónsson, H. A climbing image nudged elastic band method for finding saddle points and minimum energy paths. *J. Chem. Phys.* **113**, 9901-9904 (2000).

16 Henkelman, G. & Jónsson, H. Improved tangent estimate in the nudged elastic band method for finding minimum energy paths and saddle points. *J. Chem. Phys.* **113**, 9978-9985 (2000).

17 Liu, X.-Z., Li, Q., Egberts, P. & Carpick, R. W. Nanoscale adhesive properties of graphene: the effect of sliding history. *Adv. Mater. Interfaces* **1**, 1300053 (2014).